IEEE Access
Multidisciplinary | Rapid Review | Open Access Journal

Received March 3, 2020, accepted April 3, 2020, date of publication April 8, 2020, date of current version April 21, 2020.

*Digital Object Identifier 10.1109/ACCESS.2020.2986607*

# An Improved Method for NURBS Free-Form Surface Based on Discrete Stationary Wavelet Transform

**DEMING KONG[1,2], XIAOQIANG TIAN[3], DEHAN KONG[3], XIAODAN ZHANG[3], AND LI YUAN[3]**

[1]Institute of Electrical Engineering, Yanshan University, Qinhuangdao 066004, China
[2]Department of Telecommunications and Information Processing, Ghent University, 9000 Ghent, Belgium
[3]Institute of Information Science and Engineering, Yanshan University, Qinhuangdao 066004, China

Corresponding author: Xiaoqiang Tian (xiaoqiangtian@yeah.net)

This work was supported in part by the National Science and Technology Major Project of the Ministry of Science and Technology of China under Grant 2017ZX05019001-011, in part by the National Natural Science Foundation of China under Grant 61501394, and in part by the Natural Science Foundation of Hebei Province of China under Grant F2016203155.

**ABSTRACT** In order to improve fitting accuracy of free-form surface, an improved method for the currently recognized NURBS free-form surface based on discrete stationary wavelet transform is proposed. Firstly, the elevation image of the free-form surface point cloud and the elevation sequence of the elevation image are obtained by using the grid method. Then, feature points of the free-form surface are extracted by the discrete stationary wavelet transform. Finally, using the extracted feature points, high accuracy NURBS free-form surface is realized. Compared with the conventional NURBS method and the NURBS method based on dual-tree complex wavelet transform, the experimental results showed that the root mean squared errors of fitting results of free-form surface were deduced 77.64% and 23.16%, respectively. Therefore, the proposed method has satisfactory fitting precision.

**INDEX TERMS** 3D measurement, reverse engineering, discrete stationary wavelet transform, NURBS free-form surface.

## I. INTRODUCTION

With the development of modern industry, construction of complex free-form surface model has been widely used in reverse engineering in recent years [1], [2]. High precision fitting of the free-form surface is an important technique for the reverse engineering and the machinery parts processing industry, and the precision level of fitting directly determines the quality of the product. Therefore, high precision fitting of the free-form surface has become increasingly important in the process of production. With the improvement of process technology, objects composed of free-form surface are widely existed in nature, daily life and various industry applications. However, the external shape of most free-form surface cannot be expressed by accurate analytical function. So, during production and processing to it, the more popular algorithm is a two-level implicit function interpolation based on center reduction [3], [4]. Point cloud of model is approximated by interpolating in the coarse scale. Then, the surface is fitted with free-form surface in the fine scale and it sums up the coarse surface and the fine surface. This method can realize surface reconstruction and reserve the fidelity of surface. But when there are more points of point cloud for fitting, surface fitting requires multiple interpolation and approximation in order to reduce detection error and to get more accurate results. As a result, lots of time will be consumed in such kind of fitting procedure. With the development of the industry and manufacturing, the above method is difficult to meet the rapid and accurate fitting requirement.

In order to solve the problem, Non-Uniform Rational B-Spline(NURBS) method are proposed, which uses the expression for non-uniform knot vector to construct rational b-spline function [5]. NURBS method can be provided uniform mathematical expression to standard analytic structure and free-form surface, which applicable to building various free-form surface and composite surface.

The associate editor coordinating the review of this manuscript and approving it for publication was Bo Sun.

NURBS method can be realized high precision fitting of various shape models by adjusting control points and weighted factor. In 1988 STEP/PDES selected NURBS method as the unique representation method of free parameter curve and surface. Hence, NURBS method is widely used in reverse engineering.

Discrete stationary wavelet transform is a time-frequency analysis method with good redundancy and shift invariance [6], [7], so it is widely used in boundary extraction [8], [9]. However, the use of the discrete stationary wavelet transform in the NURBS free-form surface has not yet been published before. This paper deals with elevation sequence of free-form surface by citing the discrete stationary wavelet transform, and a series of wavelet detail coefficients can be obtained. According to the above a series of wavelet detail coefficients, feature points are extracted. In order to determine the shape of the curve between adjacent feature points, the points on the curve between two adjacent feature points are selected by using the circumferential method. The selected points above and the feature points compose date points. Control points of the NURBS free-form surface are obtained according to the inverse operation of date points. High precision fitting is realized by using the control points.

The novelty of this paper includes: the discrete stationary wavelet transform is initially introduced into NURBS free-form surface. Because the discrete stationary wavelet transform has fast mathematical calculation, redundancy and shift invariance, the feature points can be quickly and accurately obtained. Based on the feature points, the high-precision NURBS free-form surface was realized.

## II. NURBS FREE-FORM SURFACE IMPROVEMENT PROCESS

### A. GRID PROCESSING OF POINT CLOUD

Using high-precision 3D scanner, point cloud of free-form surface is acquired in 3D space. Points of acquired point cloud are irregular and disordered. To facilitate the application of the discrete stationary wavelet transform to study points of acquired point cloud, points of acquired point cloud are meshed [10], [11].

Firstly, boundary size of point cloud of free-form surface can be obtained by searching for the maximum value of X axis-direction and Y axis-direction. Then, the largest rectangle or square is acquired according to boundary size. Finally, smaller rectangles or squares are classified along the X axis-direction and Y axis-direction, as shown in (1)-(2). Suppose the length and width of rectangle or square are $Q_x$ and $Q_y$.

$$V_m = (x_{\max} - x_{\min}) \Big/ Q_x, \quad V_m \in N^* \tag{1}$$

$$V_n = (y_{\max} - y_{\min}) \Big/ Q_y, \quad V_n \in N^* \tag{2}$$

where $x_{max}$ and $x_{min}$ are the maximum and minimum value of X axis-direction, $y_{max}$ and $y_{min}$ are the maximum and minimum value of Y axis-direction, respectively. V$m$ is the number of grids of X axis-direction. V$n$ is the number of grids of Y axis-direction.

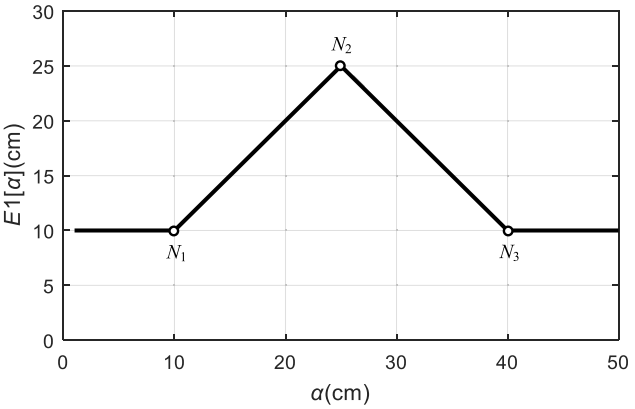


**FIGURE 1.** Elevation sequence of triangle.

To make the resolution of the elevation image more specific, the total number of grids is greater than or equal to the total number of points of point cloud. Elevation values of grids can be obtained by using the interpolation method. The equidistant grids are taken as the pixel points in an image, and then the elevation values of the grids are taken as the elevation values of the pixel points, that is, the elevation image of the point cloud of the free-form surface in the XY plane is obtained.

### B. DISCRETE STATIONARY WAVELET TRANSFORM AND FEATURE POINT EXTRACTION

In the XY plane, the point cloud is transformed into elevation sequence by using the gridding method presented in Section II(A). The elevation sequence may include the distribution of triangle, sphere, elliptical, etc. so the proposed method makes a study of the NURBS free-form surface based on discrete stationary wavelet transform by taking the distribution of triangle as the example. The elevation sequence of triangle can be obtained and denoted by $E_1[\alpha]$.

$$E_1[\alpha] = \sum_{r_1=1}^{M} C_1 \delta[\alpha - r_1] + \sum_{r_1=N_1}^{N_2-1} G_1 (r_1 - N_1) \delta[\alpha - r_1] + \sum_{r_2=N_2}^{N_3} [G_1 (N_2 - N_1) + G_2 (r_2 - N_2) \delta[\alpha - r_2]] \tag{3}$$

where $\delta[\alpha]$ is unit pulse signal, $\alpha \in [1, M]$; $M$ is the number of grid points in elevation sequence; $C_1$ is the elevation of bottom face; $G_1$ and $G_2$ are the gradients of triangle; $N_1$, $N_2$ and $N_3$ are the feature points of triangle; The graph corresponding to the (3) is shown in Fig. 1.

The elevation sequence of the triangle is analyzed by using the discrete stationary wavelet transform [12], [13], and elevation variation in the elevation sequence is extracted. In order to extract the elevation variation in the elevation sequence of the triangle, the "db1" wavelet basis is chosen

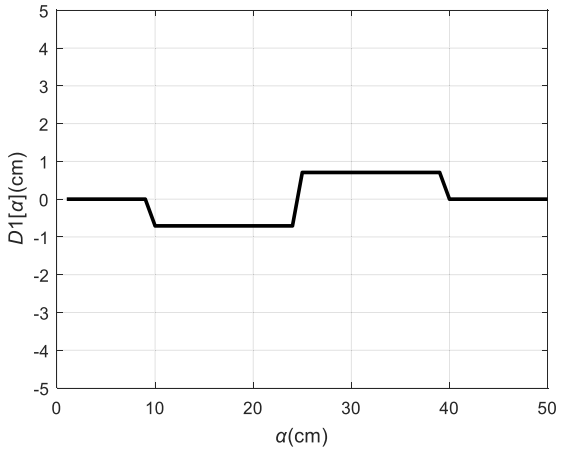


**FIGURE 2.** Wavelet detail coefficient of elevation sequence.

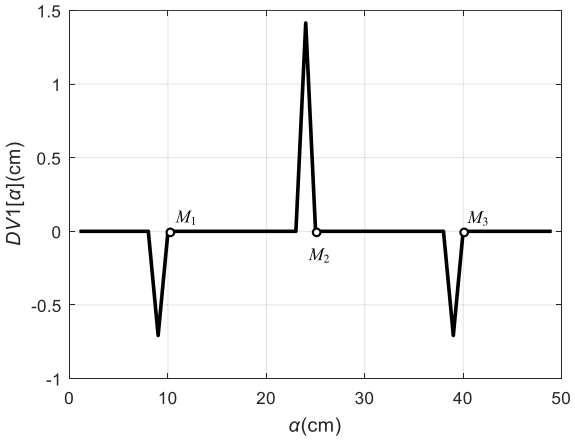


**FIGURE 3.** Adjacent wavelet detail coefficient of elevation sequence.

to extract it. The elevation sequence of triangle is processed by selecting the suitable low pass filter and high pass filter of the discrete stationary wavelet transform.

$$\begin{cases} A = h \otimes E \\ D = g \otimes E \end{cases} \tag{4}$$

where $E$ is the elevation sequence, $h$ is the low pass filter, $g$ is the high pass filter, $\otimes$ is the convolution computation, $A$ is the first-level wavelet approximation coefficient, $D$ is the wavelet detail coefficient. By applying the property of the discrete stationary wavelet transform, the elevation variation in the elevation sequence of triangle exists in wavelet detail coefficient, $D_1[\alpha]$, as shown in (5).

$$D_1[\alpha] = \varepsilon \left\{ -G_1 \sum_{r_1=N_1}^{N_2-1} \delta[\alpha - r_1] - G_2 \sum_{r_2=N_2}^{N_3} \delta[\alpha - r_2] + [G_1(N_2 - N_1) + G_2(N_3 - N_2)]\,\delta[\alpha - N_3] \right\} \tag{5}$$

The graph corresponding to the (5) is shown in Fig. 2.

In order to more accurately acquire the periphery of triangle, the difference between adjacent wavelet detail coefficient is calculated by using (6).

$$DV_1[\alpha] = D_1[\alpha] - D_1[\alpha - 1] \tag{6}$$

The distribution of the difference between adjacent wavelet detail coefficient is shown in Fig. 3.

Compared with discrete wavelet transform, the discrete stationary wavelet transform possesses not only fast mathematical calculation, but also redundancy and translation invariance. The translation invariance is that the length of the wavelet detail coefficient is identical to the length of original signal. Then, according to the corresponding time shift parameter, boundary points can be quickly and accurately determined in the original signal. As the distribution of the difference between adjacent wavelet detail coefficient is analyzed in Fig. 3, the waveform of the position of the boundary points are shown as shock signal. Because the discrete stationary wavelet transform uses linear filter, the elevation value of triangle can be calculated according to the amplitude of the shock signal. Position of shock signal ($M_1$, $M_2$ and $M_3$) in Fig. 3 are identical with the positon of boundary points ($N_1$, $N_2$ and $N_3$) of original signal in Fig. 1. Therefore, the boundary points of original signal are extracted by the position of shock signal, and the boundary points of original signal as the feature points of the triangle.

### C. NURBS FREE-FORM SURFACE IMPROVEMENT PROCESS

Because the shape of the curve is unknown, the shape of the between adjacent feature points cannot be determined by coordinate information of feature points. Therefore, the points are selected between adjacent feature points by using the circumcircle method. Firstly, three adjacent feature points are selected to make a circumcircle from left to right along the X-axis. The equation of circumcircle can be expressed as:

$$x^2 + z^2 + Gx + Iz + F = 0 \tag{7}$$

The center of a circumcircle is $(G/2, I/2)$. Then, the average angle of the line between feature point, $Q_i$ $(x_i, z_i)$, and center point can be calculated by using the (8)-(9).

$$\Delta z_i = z_i - G/2, \quad \Delta x_i = x_i - I/2 \tag{8}$$

$$\begin{cases} \theta_i = \arctan\left|\dfrac{\Delta z_i}{\Delta x_i}\right|, & \Delta z_i > 0,\ \Delta x_i > 0 \\ \theta_i = \arctan\left|\dfrac{\Delta z_i}{\Delta x_i}\right| + \dfrac{\pi}{2}, & \Delta z_i > 0,\ \Delta x_i < 0 \\ \theta_i = \arctan\left|\dfrac{\Delta z_i}{\Delta x_i}\right| + \pi, & \Delta z_i < 0,\ \Delta x_i < 0 \\ \theta_i = \arctan\left|\dfrac{\Delta z_i}{\Delta x_i}\right| + \dfrac{3\pi}{2}, & \Delta z_i < 0,\ \Delta x_i > 0 \end{cases} \tag{9}$$

Points can be selected on the curve between adjacent feature points. The central angle of selected points can be

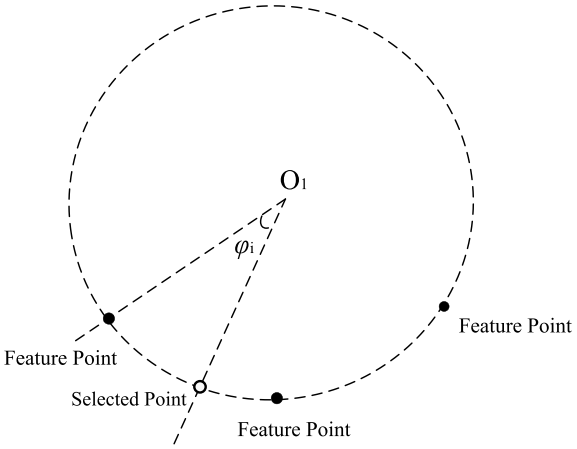


**FIGURE 4.** Selection points between adjacent feature points.

expressed as:

$$\begin{cases} \varphi_i = \dfrac{|\theta_i - \theta_{i+1}|}{n+1}, & 0 \le |\theta_i - \theta_{i+1}| < \pi \\ \varphi_i = 2\pi - \dfrac{|\theta_i - \theta_{i+1}|}{n+1}, & \pi \le |\theta_i - \theta_{i+1}| < 2\pi \end{cases} \tag{10}$$

The slope of the average angle can be calculated by using the (11).

$$k_{ij} = \tan(\theta_i - n\varphi_i) \tag{11}$$

As the shape of the curve between adjacent feature points is unknown, the slope of the line between point on the fitting curve and center point can be expressed as:

$$k' = \frac{z - E/2}{x - G/2} \tag{12}$$

By comparing the values of $k$ and $k'$, the points are selected between adjacent feature points, as shown in Fig. 4.

The selected points in Section II(C) and the obtained feature points in Section II(B) compose date points. Control points of the NURBS free-form surface are obtained according to the inverse operation of date points. NURBS free-form surface of $(p, q)$ order is constructed from many curves in the direction of $u$ and $v$. The equation of the NURBS free-form surface can be expressed as [14].

$$S(u, v) = \frac{\sum_{i=0}^{m}\sum_{j=0}^{n} N_{i,p}(u)N_{j,q}(v)\omega_{i,j}CP_{i,j}}{\sum_{i=0}^{m}\sum_{j=0}^{n} N_{i,p}(u)N_{j,q}(v)w_{i,j}}, \quad 0 \le u, v \le 1 \tag{13}$$

where $CP_{i,j}$ is the control points; $w_{i,j}$ is the weighted factor; $N_{i,p}(u)$ is B-spline basis function of $p$ order in the direction of u; $N_{j,q}(v)$ is B-spline basis function of $q$ order in the direction of $v$. Node vector $U$ and node vector $V$ can be calculated by using the deBoor-eox recurrence (14).

$$\begin{cases} U = \left\{0, \underset{p+1}{\cdots}, 0, u_{p+1}, \cdots, u_{r-p-1}, 1, \underset{p+1}{\cdots}, 1\right\} \\ V = \left\{0, \underset{q+1}{\cdots}, 0, u_{q+1}, \cdots, u_{s-q-1}, 1, \underset{q+1}{\cdots}, 1\right\} \end{cases} \tag{14}$$

where $r = p + m + 1$ and $s = q + n + 1$. Node number of node vector $U$ and node vector $V$ are $(r + 1)$ and $(s + 1)$, respectively.

Inverse operation of NURBS free-form surface refers to construct a NURBS free-form surface of $(p, q)$ order. Interpolate the surface with the topological rectangle date points, and the date points are $Q_{k,l}, k = 0, 1, \ldots, m; l = 0, 1, \ldots, n$. The inverse operation of NURBS free-form surface can also be represented as solving linear equations of unknown control points as well as the inverse operation of NURBS curve, and the control points are $CP_{i,j}(i = 0, 1, \ldots, m + p - 1; j = 0, 1, \ldots, n + q - 1)$. In general, the first and the last points of the curve in the direction of $u$ and $v$ are consistent with the first and the last date points. There is a one-to-one correspondence between date points and nodes of free-form surface [15]. To determine the node values corresponding to the data points, data points are parameterized by using the parametrization method of accumulating chord length. Parameterization of chord length can be calculated by using the (15)-(16) in the direction of $u$ [16], [17].

$$d = \sum_{k=1}^{m} |Q_k - Q_{k-1}| \tag{15}$$

$$\begin{cases} u'_0 = 0 \\ u'_k = u'_{k-1} + \dfrac{|Q_k - Q_{k-1}|}{d}, \quad k = 1, 2, \cdots, m-1 \end{cases} \tag{16}$$

where $d$ is total chord length, $u'_k$ is the node parameter value of $Q_k$. Appropriate node vector $U$ can be selected by using the averaging method in (16), and the linear equations of coefficient matrix can be expressed as:

$$\begin{cases} u_0 = \cdots = u_p = 0, \quad u_{r-p} = \cdots = u_r = 1 \\ u_{i+p} = \dfrac{1}{p}\sum_{k=i}^{j+p-1} u'_k, \quad i = 1, 2, \cdots m - p \end{cases} \tag{17}$$

The linear equations of interpolation NURBS free-form surface can be written as:

$$Q_{k,l} = \sum_{i=0}^{m}\sum_{j=0}^{n} N_{i,2}(u'_k)N_{j,2}(v'_l)CP_{i,j} \tag{18}$$

$$\begin{cases} N_{i,0}(u'_k) = \begin{cases} 1, & u_i \le u'_k \le u_{i+1} \\ 0, & others \end{cases} \\ N_{i,2}(u'_k) = AN_{i,0}(u'_k) + BN_{i+1,0}(u'_k) + CN_{i+2,0}(u'_k) \end{cases} \tag{19}$$

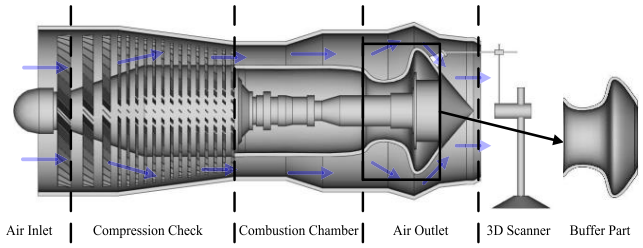


**FIGURE 5.** A schematic diagram for a type of automobile engine.

where

$$\begin{cases} A = \dfrac{(u'_k - u_i)^2}{(u_{i+2} - u_i)(u_{i+1} - u_i)} \\ B = \dfrac{(u_{i+2} - u'_k)(u'_k - u_i)}{(u_{i+2} - u_{i+1})(u_{i+2} - u_i)} + \dfrac{(u_{i+3} - u'_k)(u'_k - u_{i+1})}{(u_{i+3} - u_{i+1})(u_{i+2} - u_{i+1})} \\ C = \dfrac{(u_{i+3} - u'_k)^2}{(u_{i+3} - u_{i+1})(u_{i+3} - u_{i+2})} \\ \dfrac{0}{0} = 0. \end{cases}$$

Node parameter value $u'_k$ and $u_i$ can be calculated by using the (16)-(17). Substitute $u'_k$ and $u_i$ into the (19). The B-spline basis function can be obtained in the node vector $U$. Substitute the B-spline basis function and the date point $Q_{k,l}$ into the (18). The B-spline basis function can be calculated by using the equation (19) in the node vector $V$. So the control points $CP_{i,j}$ of the NURBS free-form surface are obtained according to the inverse operation of date points [18]. High precision NURBS free-form surface is realized according to the control points, node vector $U$ and node vector $V$.

## III. EXPERIMENTAL AND SIMULATION STUDY

### A. FREE-FORM SURFACE OF AEROENGINE BUFFER SIMULATION PROCESS

A schematic diagram for a type of aeroengine is shown in Fig. 5 [19], [20]. Part of the aeroengine buffer is composed of the free-form surface. which is located in the air outlet of the aeroengine. Since the 3D scanner can scan the part of the aeroengine buffer made up of the free-form surface by going into the aeroengine, high precision point cloud of the measured object was obtained by high-precision scanning. The free-form surface of the air outlet of the aeroengine can be detected and generated by using the proposed method. The specific simulation process is as follows: In order to verify the feasibility of the proposed method, simulation mode was selected as simulation study of the free-form surface in the air outlet of the aeroengine. Point cloud of the free-form surface was showed in Fig. 6.

### B. GRID PROCESSING OF FREE-FORM SURFACE AND FEATURE POINT EXTRACTION

Grid of the point cloud of the free-form surface was constructed by using the gridding method presented in Section II(A), as shown in Fig. 7.

According to the result of the grid processing, the points of the free-form surface were divided into the elevation

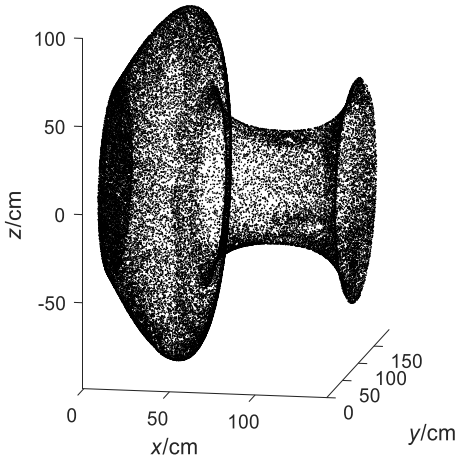


**FIGURE 6.** Point cloud of the free-form surface.

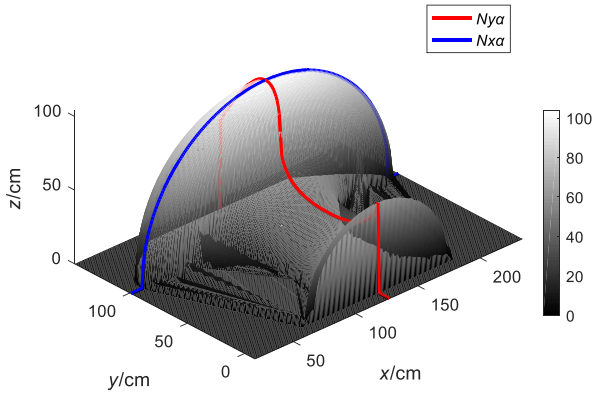


**FIGURE 7.** Constructed grid of the free-form surface.

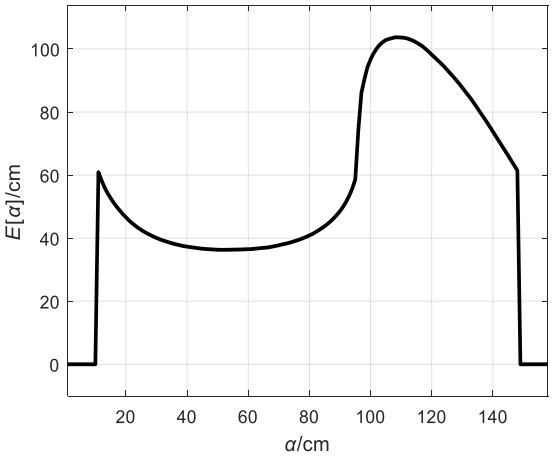


**FIGURE 8.** Elevation sequence of $Ny\alpha$.

sequences of X axis-direction and the elevation sequences of Y axis-direction. The sum of each elevation sequences of X axis-direction and Y axis-direction were calculated. The maximum of the sum of elevation sequence were selected and denoted by $Nx\alpha$ and $Ny\alpha$, as shown in Fig. 8 and Fig. 9, respectively.

The discrete stationary wavelet transform was carried out on the elevation sequences of the free-form surface.

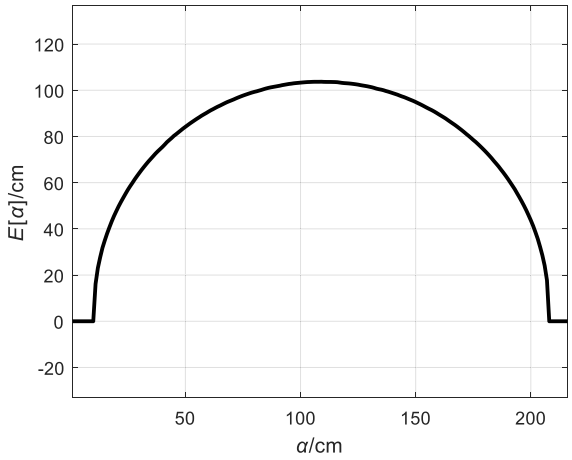


**FIGURE 9.** Elevation sequence of *Nxα*.

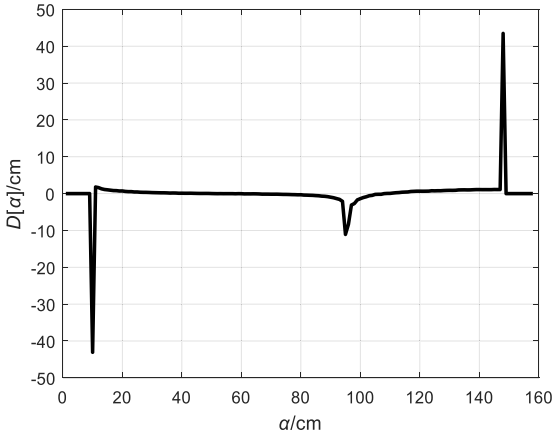


**FIGURE 10.** Wavelet detail coefficient of *Nyα*.

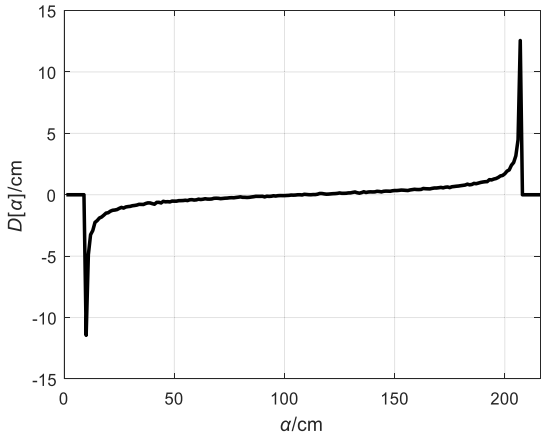


**FIGURE 11.** Wavelet detail coefficient of *Nxα*.

The elevation sequences of *Nxα* and *Nyα* corresponding wavelet detail coefficient were obtained, as shown in Fig. 10 and Fig. 11, respectively.

In order to more accurately acquire the periphery of the free-form surface, the difference between adjacent wavelet detail coefficients of *Nxα* and *Nyα* were calculated by using the (6), as shown in Fig. 12 and Fig. 13, respectively.

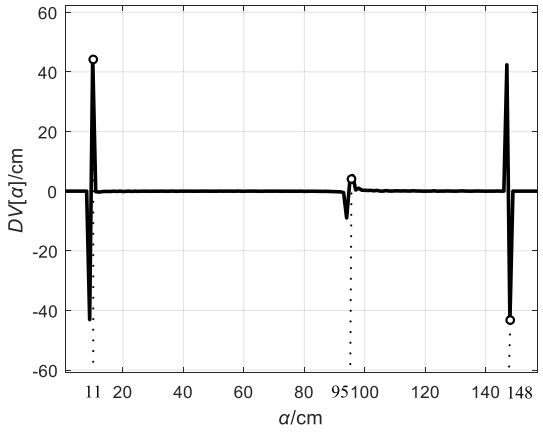


**FIGURE 12.** Adjacent wavelet detail coefficient of *Nyα*.

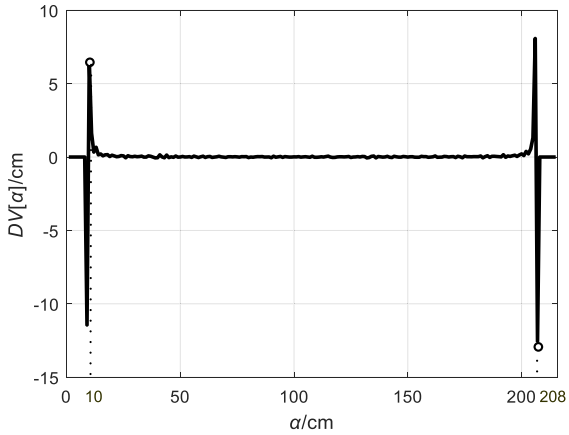


**FIGURE 13.** Adjacent wavelet detail coefficient of *Nxα*.

According to the Fig. 13, position of shock signal of the *Nxα* corresponding discrete sequence were 10 and 208. Position of shock signal of the *Nyα* corresponding discrete sequence were 11, 95 and 148 based on the Fig. 12. According to the relationship between the position of shock signal and the position of boundary points in Section II(B), the boundary points ($Q_1$, $Q_3$, and $Q_5$), the highest point in the discrete sequence *Nyα* ($Q_2$) and the lowest point in the discrete sequence *Nyα* ($Q_4$) as the feature points of the free-form surface. The coordinate values of feature points are shown in the Table 1.

### C. FITTING RESULTS OF PROPOSED METHOD

Points were selected between adjacent feature points by using the circumcircle method presented in Section II(C). The feature points of the free-form surface were divided into two groups from left to right along the X-axis, each of which were adjacent feature points. Substitute the coordinate values of two groups of feature points into the (7). Circumcircle equation coefficient can be obtained as:

$$\begin{cases} G_1 = 107.378, & I_1 = 170.965 \\ G_2 = 241.341, & I_2 = 151.278 \end{cases} \tag{20}$$

The centers of circumcircle were $O_1$(53.689, 85.483) and $O_2$(120.671, 75.639) based on the (20).

**TABLE 1.** Coordinate values of feature points.

| | $Q_1$ | $Q_2$ | $Q_3$ | $Q_4$ | $Q_5$ |
|---|---|---|---|---|---|
| $x$/cm | 11 | 51 | 95 | 108 | 148 |
| $y$/cm | 109 | 109 | 109 | 109 | 109 |
| $z$/cm | 60.89 | 36.29 | 58.64 | 103.7 | 61.46 |

**TABLE 2.** Coordinate values of feature points.

| | $Q_6$ | $Q_7$ | $Q_8$ | $Q_9$ |
|---|---|---|---|---|
| $x$/cm | 25 | 93 | 102 | 120 |
| $y$/cm | 109 | 109 | 109 | 109 |
| $z$/cm | 42.61 | 53.44 | 100.1 | 98.2 |

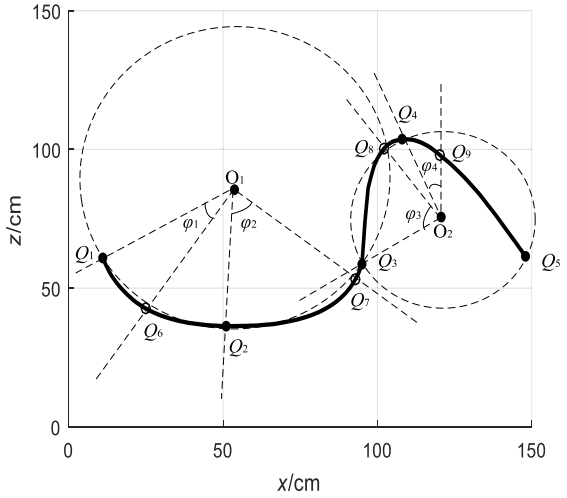


**FIGURE 14.** Selection points between adjacent feature points of free-form surface.

Position of points ($Q_6$, $Q_7$, $Q_8$ and $Q_9$) were solved by using the method presented in Section II(C), as shown in Fig. 14. The coordinate values of the points are shown in the Table 2.

The selected points above and the feature points compose date points. Using the (16)-(19), the control points, node vector U and node vector V of NURBS free-form surface were calculated. High precision NURBS free-form surface is realized based on the control points and the B-spline basis function, as shown in Fig. 15.

### D. FITTING RESULTS OF PROPOSED METHOD

Because conventional NURBS method cannot extract feature points, the required fitting points were selected by using the equal spacing method. The coordinate values of the fitting points are shown in the Table 3. The fitting result of the conventional NURBS method were shown in Fig. 16.

Because NURBS method based on dual-tree complex wavelet transform(DTCWT-NURBS method) has the characteristic of shift invariance, it can be used to extract feature points. The elevation sequences of $Nx\alpha$ and $Ny\alpha$ were processed by using the dual-tree complex wavelet transform,

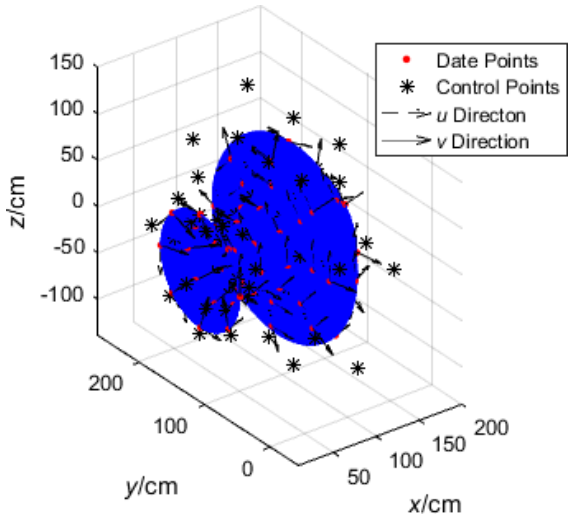


**FIGURE 15.** Fitting results of proposed method.

**TABLE 3.** Coordinate values of the fitting points.

| | $Q_1$ | $Q_2$ | $Q_3$ | $Q_4$ | $Q_5$ | $Q_6$ | $Q_7$ | $Q_8$ | $Q_9$ |
|---|---|---|---|---|---|---|---|---|---|
| $x$/cm | 11 | 28 | 45 | 63 | 80 | 97 | 114 | 131 | 148 |
| $y$/cm | 109 | 109 | 109 | 109 | 109 | 109 | 109 | 109 | 109 |
| $z$/cm | 60.89 | 40.98 | 36.64 | 36.74 | 40.88 | 86.08 | 102.6 | 86.47 | 61.46 |

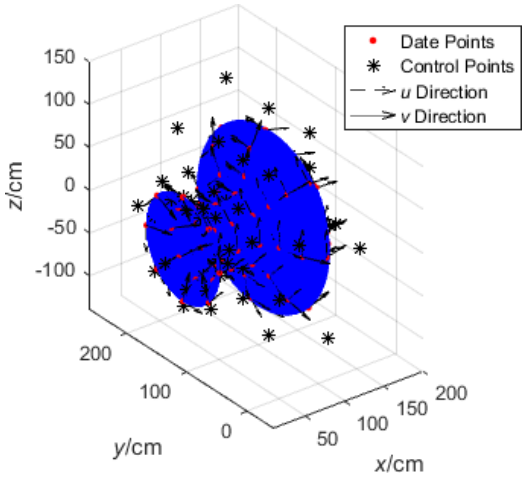


**FIGURE 16.** Fitting results of conventional NURBS method.

and the wavelet detail coefficient were obtained, as shown in Fig. 17 and Fig. 18, respectively.

According to the relationship between the position of shock signal and the position of boundary points, the boundary points were obtained. The coordinate values of the fitting points are shown in the Table 4. The fitting result of the DTCWT-NURBS method were shown in Fig. 19.

To illustrate fitting effect of the proposed method, the fitting results of the conventional NURBS method, the DTCWT-NURBS method and the proposed method were

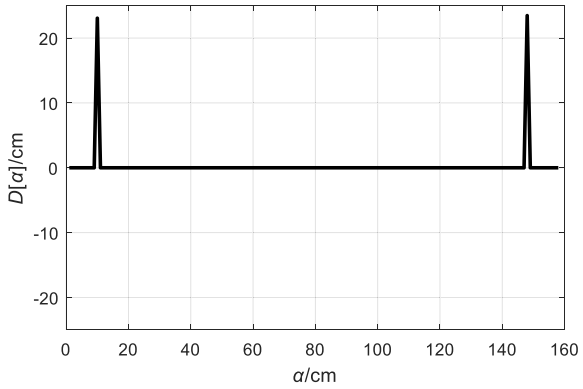


**FIGURE 17.** Wavelet detail coefficient of *Nyα*.

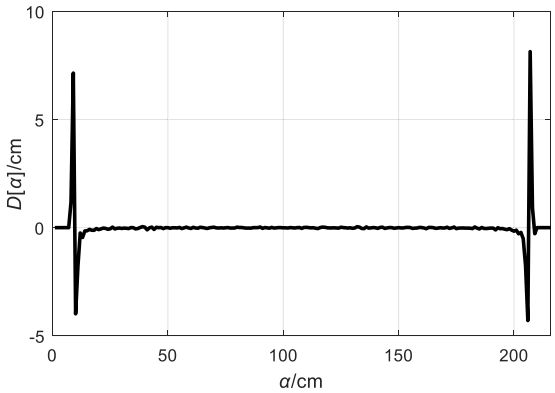


**FIGURE 18.** Wavelet detail coefficient of *Nxα*.

**TABLE 4.** Coordinate values of the fitting points.

| | $Q_1$ | $Q_2$ | $Q_3$ | $Q_4$ | $Q_5$ | $Q_6$ | $Q_7$ | $Q_8$ | $Q_9$ |
|---|---|---|---|---|---|---|---|---|---|
| *x*/cm | 11 | 27 | 51 | 87 | 94 | 104 | 108 | 130 | 148 |
| *y*/cm | 109 | 109 | 109 | 109 | 109 | 109 | 109 | 109 | 109 |
| *z*/cm | 60.89 | 41.46 | 36.29 | 45.4 | 55.66 | 102.2 | 103.7 | 87.72 | 61.46 |

**TABLE 5.** Average values of error of mean square root above THREE methods.

| | Average value of error of mean square root /cm | | |
|---|---|---|---|
| | Conventional NURBS Method /cm | DTCWT-NURBS Method /cm | Proposed Method /cm |
| Free-form surface | 0.4213 | 0.1226 | 0.0942 |

compared by using error of mean square root. When *y* equals 109, different *y* corresponding to *z* in the fitting results of above three methods and standard values were obtained and shown in Fig. 20. The error of mean square root was calculated by using the (21), as shown Fig. 21.

$$RE = \sqrt{\sum (AE_i)^2 / n} \tag{21}$$

where $AE_i$ is error value.

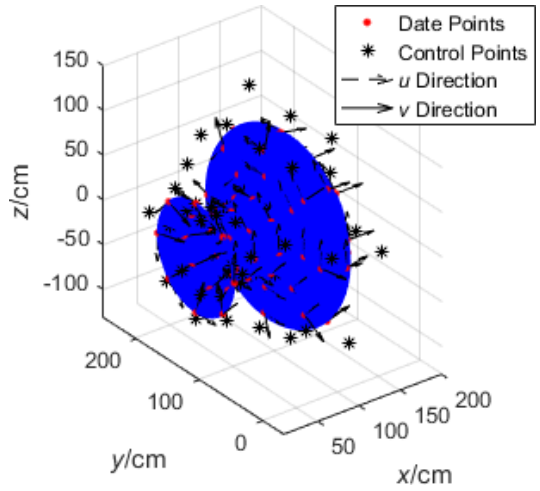


**FIGURE 19.** Fitting results of DTCWT-NURBS method.

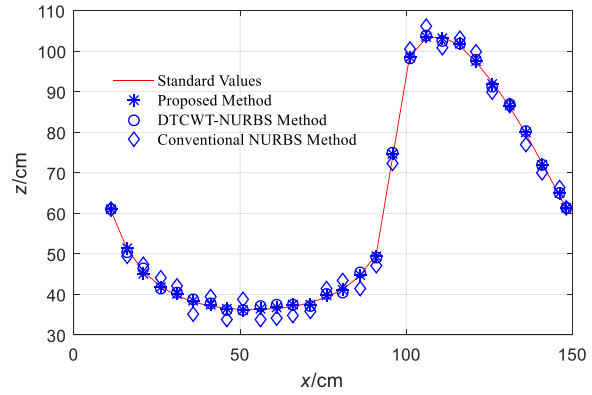


**FIGURE 20.** Fitting results of *y* equals 109 by using conventional NURBS method, DTCWT-NURBS method and proposed method.

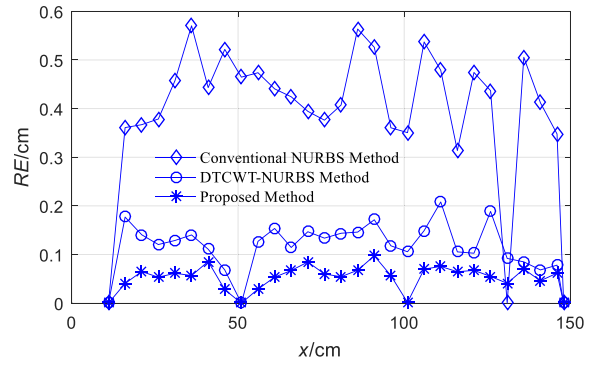


**FIGURE 21.** Absolute errors of NURBS free-form surface by using conventional NURBS method, DTCWT-NURBS method and proposed method.

The point cloud of the free-form surface was calculated by using the error of mean square root. Average values of error of mean square root above three methods were obtained and listed in Table 5.

On the basis of the Table 5 above, it can be seen that the average absolute errors by using the conventional NURBS method, the DTCWT-NURBS method and the proposed method were 0.4213, 0.1226 and 0.0942, respectively.

Compared to the conventional NURBS method and the DTCWT-NURBS method, the average absolute errors were reduced by 77.64% and 23.16%, respectively. And hence, the proposed method can realize the high-precision NURBS free-form surface.

## IV. CONCLUSION

In this study, a novel method is proposed to improve fitting accuracy of free-form surface. Compared with the conventional NURBS method and the DTCWT-NURBS method, a more satisfactory fitting result can be obtained for the free-form surface by using the proposed method. In order to verify the feasibility of the proposed method, simulation mode was selected as simulation study of the free-form surface in the air outlet of the aeroengine. The experiment results show that the proposed method is more promising than the existing method in the field of the NURBS free-form surface.

## REFERENCES


[1] F. Wu, J. Li, H. Yang, P. Yang, J. Liu, X. Liang, and B. Yuan, "Research of pavement topography based on NURBS reconstruction for 3D structured light," *Optik*, vol. 194, Oct. 2019, Art. no. 163074.

[2] L. Zhang, S. Zhou, D. Li, Y. Liu, T. He, B. Yu, and J. Li, "Pure adaptive interferometer for free form surfaces metrology," *Opt. Express*, vol. 26, no. 7, pp. 7888–7898, Apr. 2018.

[3] J. Reimers, A. Bauer, K. P. Thompson, and J. P. Rolland, "Freeform spectrometer enabling increased compactness," *Light: Sci. Appl.*, vol. 6, no. 7, pp. e17026–e17026, Jul. 2017.

[4] J. Zhang, J. Hou, and T. T. Wu, "Fast surface reconstruction algorithm for 3D scattered point cloud model," *J. Comput.-Aided Des. Comput. Graph.*, vol. 30, no. 2, pp. 235–243, Feb. 2018.

[5] E. Zieniuk and K. Szerszen, "NURBS curves in direct definition of the shapes of the boundary for 2D Stokes flow problems in modified classical BIE," *Appl. Numer. Math.*, vol. 132, pp. 111–126, Oct. 2018.

[6] H. Xu, H. Li, X. Yang, S. Qi, and J. Zhou, "Integration of terrestrial laser scanning and NURBS modeling for the deformation monitoring of an Earth-rock dam," *Sensors*, vol. 19, no. 1, p. 22, 2019.

[7] L. Xu, D. Kong, and X. Li, "On-the-Fly extraction of polyhedral buildings from airborne LiDAR data," *IEEE Geosci. Remote Sens. Lett.*, vol. 11, no. 11, pp. 1946–1950, Nov. 2014.

[8] D. Kong, L. Xu, X. Li, and S. Li, "K-Plane-Based classification of airborne LiDAR data for accurate building roof measurement," *IEEE Trans. Instrum. Meas.*, vol. 63, no. 5, pp. 1200–1214, May 2014.

[9] A. V. Leonov, M. N. Anikushkin, and A. V. Ivanov, "Laser scanning and 3D modeling of the Shukhov hyperboloid tower in Moscow," *J. Cultural Heritage*, vol. 16, no. 4, pp. 551–559, Aug. 2015.

[10] M. Hoffmann, D. Haering, and M. Begon, "Comparison between line and surface mesh models to represent the rotator cuff muscle geometry in musculoskeletal models," *Comput. Methods Biomech. Biomed. Eng.*, vol. 20, no. 11, pp. 1175–1181, Aug. 2017.

[11] K.-D. Bouzakis, D. Pantermalis, I. Mirisidis, M. Grigoriadou, E. Varitis, A. Sakellaridou, A. Bouzaki, K. Efstathiou, S. Theodoridou, A. Papacharisi, and E. Diamanti, "3D-laser scanning of the parthenon west frieze blocks and their digital assembly based on extracted characteristic geometrical details," *J. Archaeol. Sci., Rep.*, vol. 6, pp. 94–108, Apr. 2016.

[12] H. Demirel and G. Anbarjafari, "IMAGE resolution enhancement by using discrete and stationary wavelet decomposition," *IEEE Trans. Image Process.*, vol. 20, no. 5, pp. 1458–1460, May 2011.

[13] H. Demirel and G. Anbarjafari, "A new sequence similarity analysis method based on the stationary discrete wavelet transform," *BMC Bioinf.*, vol. 19, no. 1, p. 165, May 2018.

[14] B. Zhou, J. Zhao, L. Li, and R. Xia, "NURBS curve interpolation algorithm based on tool radius compensation method," *Int. J. Prod. Res.*, vol. 54, no. 15, pp. 4448–4474, Aug. 2016.

[15] M. Duan and C. Okwudire, "Minimum-time cornering for CNC machines using an optimal control method with NURBS parameterization," *Int. J. Adv. Manuf. Technol.*, vol. 85, nos. 5–8, pp. 1405–1418, Jul. 2016.

[16] D. A. Swyt, "Length and dimensional measurements at NIST," *J. Res. Nat. Inst. Standards Technol.*, vol. 106, no. 1, pp. 1–23, Jan. 2001.

[17] Z.-L. Liu and J. Yang, "Analysis of electromagnetic scattering with higher-order moment method and nurbs model," *Prog. Electromagn. Res.*, vol. 96, pp. 83–100, 2009.

[18] S. Tao, "Reverse calculating the control points of cubic B-spline curves," *Bull. Sci. Technol.*, vol. 15, no. 3, pp. 23–25, Nov. 2014.

[19] Y. B. Tang, G. H. Luo, and K. Y. Zheng, "Structure parameter design of Aeroengines," *Aeroengine*, vol. 30, no. 2, pp. 10–13, May 2004.

[20] K. B. He, L. Feng, and J. Wang, "Design of electronic chip radiator based on aero-engine blade structure," *Technol. Market*, vol. 26, no. 1, pp. 121–123, Nov. 2019.


**DEMING KONG** received the B.S. degree in electronics and communication engineering and the M.S. degree in communication and information systems from Yanshan University, China, in 2006 and 2010, respectively, and the Ph.D. degree in measurement technology and instruments from Beihang University, China, in 2015. He worked as a Visiting Scholar with Ghent University, from 2018 to 2019, where he is currently an Associate Professor with the College of Electrical Engineering. He is mainly working on high precision 3D shape detection technology.

**XIAOQIANG TIAN** received the B.S. degree in measurement and control technology from Liren College, Yanshan University, China, in 2013, through the Instrumentation Program, and the M.S. degree in instrument and meter engineering from the Kunming University of Science and Technology, China, in 2016, where he is currently pursuing the Ph.D. degree with the College of Computer Science and Engineering. He is currently working on high precision 3D shape detection technology.

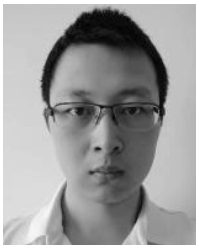

**DEHAN KONG** received the Ph.D. degree in computer science and technology from Yanshan University, China, in 2017. He is currently working on a spatial database, points cloud, and pattern recognition.

**XIAODAN ZHANG** received the B.S. degree in computer science and technology from Yanshan University, China, in 2016, where she is currently pursuing the Ph.D. degree with the College of Computer Science and Engineering. She is currently working on intelligent information processing.

**LI YUAN** received the master's degree in educational technology from Nanjing Normal University, in 2011. She is currently pursuing the Ph.D. degree in intelligent information processing with the School of Computer Science and Engineering, Yanshan University.